CHALMERS
UNIVERSITY OF TECHNOLOGY

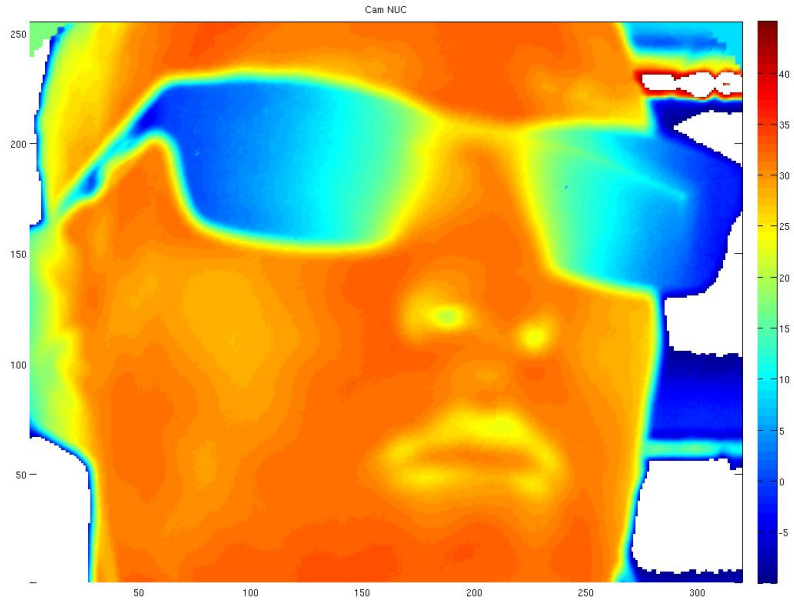

Heat Transfer Studies with IR Thermography Techniques

Master's Thesis in Solid and Fluid Mechanics

Ángel Barrachina Martín

Department of Applied Mechanics
Division of Fluid Dynamics
Chalmers University of Technology
Göteborg Sweden, 2014

Master's Thesis [2014 : 70]

Master's Thesis 2014:70

Heat Transfer Studies with IR Thermography Techniques

Master's Thesis

Ángel Barrachina Martín

Department of Applied Mechanics
Division of Fluid Dynamics
Chalmers University of Technology
Göteborg, Sweden, 2014

Heat Transfer Studies with IR Thermography Techniques
Master's Thesis
Ángel Barrachina Martín

Master's Thesis 2014:70
ISSN: 1652-8557

Department of Applied Mechanics,
Division of Fluid Dynamics
Chalmers University of Technology
Se-412 96 Göteborg, Sweden
Phone +46-(0)31-7721400
Fax: +46-(0)31-180976

Printed at Chalmers Reproservice
Göteborg, Sweden 2014

Ángel Barrachina Martín

Master's Thesis

by

Ángel Barrachina Martín
angelb@student.chalmers.se
Department of Applied Mechanics
Division of Fluid Dynamics
Chalmers University of Technology

Abstract

The work carried out that is described on this report focuses on some experimental studies involving IR thermography techniques. The first part of the study has been centered in the investigation of IR transparent materials to be implemented as a window for the Linear Cascade facility that Chalmers has in the Applied Dynamics department. The results obtained for the material chosen are compared with the optical properties that the supplier provides. The main application of these results is intended to be used in the fluid dynamics laboratory, but it can be of application in many fields as for example combustion chamber measurements.

Also, a new calibration and NUC (Non Uniformity Correction) has been made so that all the image corrections can be made automatically using MatLab code and LabView without any need of intermediate software. This will be explained more deeply in the report.

Heat transfer experiments have been done in a subsonic Linear Cascade facility to simulate the thermal behaviour of Outlet Guide Vanes (OGVs) in jet engines. These are focused on measuring the convective heat transfer coefficient (HTC). This could help us optimize the design of this section of aeroengines.

Finally, Temperature measurements have been carried out in the Linear Cascade facility using the window studied in the first part of the experiment in order to validate some correlations obtained for the transmittance of the window.

Acknowledgement

I would like to thank in first place my supervisor during this semester, Borja Rojo. His advices at any moment I needed them were of incalculable help. Also, his experience doing his Master's Thesis two years ago helped me in a very important way in order to organise all my work.

Thanks also to Carlos Jimenez, who has always been of help at any time I needed it in the lab. His knowledge and previous experience with the equipment used in this lab has always solved me many problems and showed me in which direction my experiments should go.

Many thanks to professor Valery Chernoray. In the end he was the one who gave the solution when we all together were not able to solve some of the problems that appeared. Also, I have to say that I learned a lot just by listening to his advices in the lab.

I would like to say thank also to my student colleague at the department Saul Llacer, with whom I spent most of the afternoon work in the office. Sharing some of the work with him has made the long days of hard work much more entertaining.

Finally, I have to express my gratitude to my family for all the support they have given me ever since I started school until this last year in Sweden. Without all the opportunities they gave me I would not have achieved any of my goals. Thanks to all my Erasmus friends, they have been my other family during this amazing year. Thanks also to all my friends from Madrid with whom I have shared all my best experiences before coming to Sweden.

Contents

Abstract

1 Introduction and Objective **3**
1.1 Measurement Method. IR camera and Calibration Rig 3

2 Theoretical Fundamentals **7**
2.1 Radiation 7
2.2 Conduction 9
2.3 Convection 10
2.4 Optical Properties of Materials 10

3 Literature research for IR transparent window **12**

4 Experimental Investigation of Silicon Window **17**
4.1 MWIR Transparent Silicon (Si) Window 17
4.2 Transmittance Calculation and Uncertainty 18
4.3 IR Transparent Window Implementation 20
4.4 Window Results 22
4.4.1 Angle and Temperature Dependence 23
4.4.2 Si Window behaviour in the Linear Cascade facility 28

5 Camera Setup **30**
5.1 NUC. Theory and Implementation 30
5.2 Bad Pixel Correction 32
5.3 Camera Calibration 34

6 Heat Transfer Experiment Setup And Facility **35**
6.1 Linear Cascade Rig 35
6.2 The Instrumented Vane 36
6.3 Vane Coordinate Markers 37

7 Experimental Results **38**
7.1 Image Post Processing 38
7.2 Fluent Simulations 40
7.3 Cases 42
7.3.1 Off-Design: 25 º air inlet velocity: 23 $\frac{m}{s}$ 43
7.3.2 Off-Design: -40 º air inlet velocity: 23$\frac{m}{s}$ 43
7.3.3 Off-Design: -40 º air inlet velocity: 30 $\frac{m}{s}$ 44
7.3.4 On-Design: -25 º air inlet velocity 20 $\frac{m}{s}$ 45
7.3.5 On-Design: -25 º air inlet velocity: 30 $\frac{m}{s}$ 46
7.4 Discussion and Comparison with CFD results 47
7.4.1 CFD results 47

8 Conclusions **49**

Chapter 1

Introduction and Objective

Fuel consumption is currently becoming a major concern when designing new components for aero engines. In particular, turbofan engines can achieve higher efficiencies by changing some configurations in the aircraft i.e. increasing the by pass ratio, increasing the temperature after the combustor, etc. Good heat transfer behaviour of certain components of a classic turbofan engine can also help achieve higher values of efficiency as well as a longer life for the engine. This project focuses specially in studying how can some typical experiments already developed in the facilities of our lab be improved. Our efforts have been centered in the usage of an IR camera to measure temperature distributions over surfaces in the most optimal way possible, increasing therefore the accuracy of our results.

1.1 Measurement Method. IR camera and Calibration Rig

The main system used for our experiments has been a MWIR (Medium Wave Infrared) Phoenix Camera System from FLIR Systems Inc. It has a cooled 320x256 array quantum photodetector with spectral response in the medium infrared ($3 - 5\mu m$). The camera has a Stirling cryocooling engine inside, as its detector must work at a temperature of $77K$. The photodetector type is an Indium Antimode type. In the next table the complete camera specifications are shown.

Manufacturer	Flir Systems Inc.
Model	Phoenix MWIR Camera System
Detector type	Indium Antimonide
Detector spectral response	1 µm - 5.4 µm
Filtered spectral response	3 µm - 5 µm
Format (pixel number, HxV)	320 x 256
Detector pitch	30 µm
Detector cooling	Stirling cycle
Detector temperature	77 K
Dynamic range	14 bit
Noise equivalent temperature difference (sensitivity)	25 mK
Minimum window	2 rows x 4 columns
Integration mode	Snapshot
Max frame rate full window	122 Hz.
Max frame rate minimum window	13.6 kHz
Integration time	9 µs - 16.6 ms
Output	Composite video / digital image / RS.232 camera control
Input	Sync (arm/trigger) / RS 232 camera control
Optics	25 mm f/2.3 MWIR / Janos Technology

Table 1.1: Camera specifications

The basic parameter to set for the camera to work properly in our experiment is the **integration time**. The variation of this parameter moves the distribution of counts that the detector measures closer or further from the saturation point of the camera (16384 counts), and must be set taking into account the temperature range we will be working in. In this case the integration time chosen has been $1.2ms$ following the manufacturer recommendation that states the optimal position of the pixel count level of our warmest level (50^oC) should be around 75 % of the saturation point.

As calibration device and study rig for the transparent IR window a black body has been used. The surface of this body has to be treated to maximise its emissivity so that we do not get unwanted reflections that can mean in the end bad measurements by the thermographic device. This coating for our surfaces is the paint Nexel Velvet-Coating 811-21 from Mankiewicz Gebr. & Co. This paint is a very common coating for IR applications and has already been used in some experiments already carried out in our lab. The characteristics why this paint gives good results are its high value of emissivity, the minimal variation of this value with angle and temperature, and good ageing properties. The coating has been applied using a spray gun of compressed air. The coating properties are listed in the Table 1.2 :

Property	Value	Comments
ε (emissivity)	0.973	Constant for our work range
Maximum angle for constant ε	30^o	60^o for 1 pcent drop
Thermal Conductivity	0.2 $\frac{W}{mK}$	Constant for our work range

Table 1.2: Black coating properties

The body which surface is treated to calibrate our camera consists on three copper plates screwed one on top of the other and with electric heaters placed in between the top and the middle plate. This body is isolated with a foam and cupboard cover on its top and placed upside down as shown in the figure below. The heaters are connected to a transformer, connected at the same time PID controller that let us keep the surface at the temperature we want it to be.

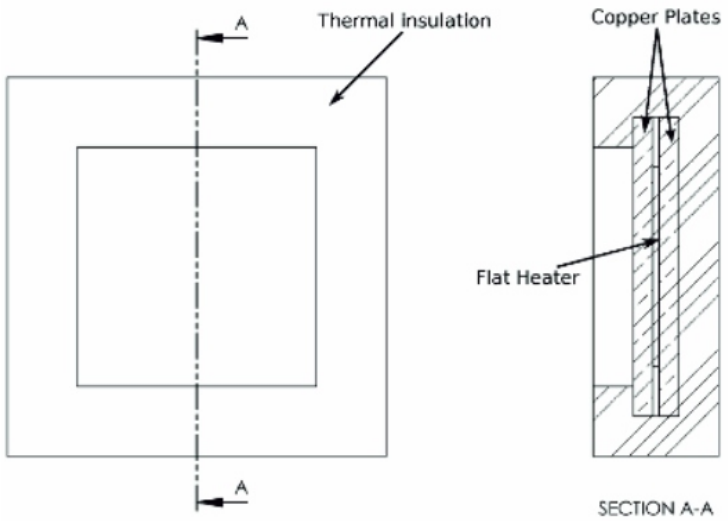

Figure 1.1: Calibration Rig Drawing

The reason for this configuration to be used is that copper is a very good thermal conductor and with the isolation on its top and side parts, an uniform distribution of temperature can be achieved in the surface facing the camera. The upside down position is used because this way we can minimise the effect of convection to the surrounding air and let the permanent state be more stable. The uniformity of the temperature in the calibration surface is really important when performing calibration and correction to the camera as it will be explained later in the report.

Between the camera and the calibration surface, a supporting device has been used to hold the IR transparent window. This device will let us change the relative angle between the camera and the window.

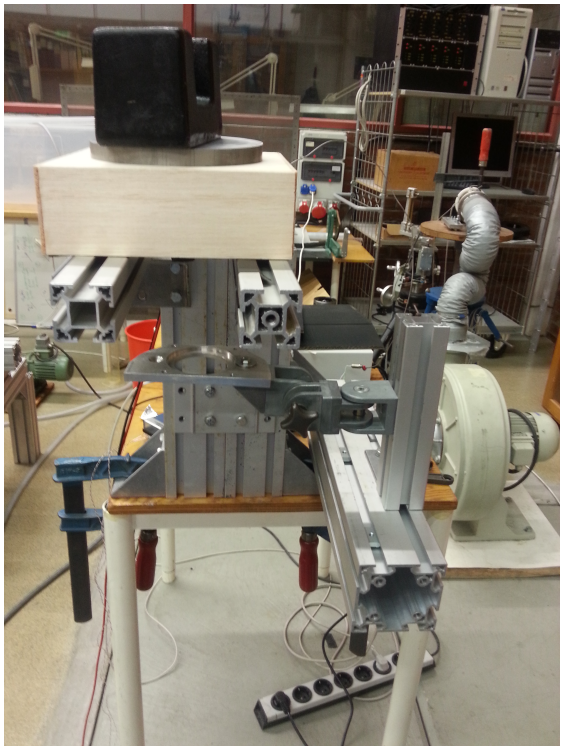

Figure 1.2: Calibration Rig

As it can be seen in Fig. 1.2, we have in between a device that will let us put the transparent medium we want to analyse

Chapter 2

Theoretical Fundamentals

To understand the phenomena analysed in this work it is important to understand the heat transfer mechanisms that always take place. These are radiation, conduction and convection. Also, it is important to understand the optical properties that have an influence in the radiative behaviour of materials

2.1 Radiation

Of these three the most important phenomenon to understand along with this work is Radiation. Thermal radiation is described as the transport of energy between bodies through photons that have specific wavelengths. Unlike the other two possible ways of heat transfer, radiation does not need matter to be transported, as energy travel as photons (waves). All concepts about thermal radiation are developed from the concept of Black Body, which is an idealization to describe a body that is able to absorb all the incident radiation that achieves him, without depending this capacity of absorption on the wavelength or the angle of incidence. Black Bodies are described mathematically by Planck distribution, which is shown below, that gives, as a function of the wavelength and the temperature of the black body the spectral radiance of the black body:

$$E_b(\lambda,T)(\frac{W}{m^3}) = \frac{C_1}{\lambda^5(e^{\frac{C_2}{\lambda T}}-1)} \tag{2.1}$$

$$C_1 = 3.742 * 10^{-16} W m^2$$

$$C_2 = 1.4385 * 10^{-2} mK$$

If we try to find where the maximum values of energy emitted occur we will find the wavelengths at which maximum values of E_b take place. These values follow the *Wien's Law*:

$$\lambda_{max} T = C_3 \tag{2.2}$$

$$C_3 = 0.002898mK$$

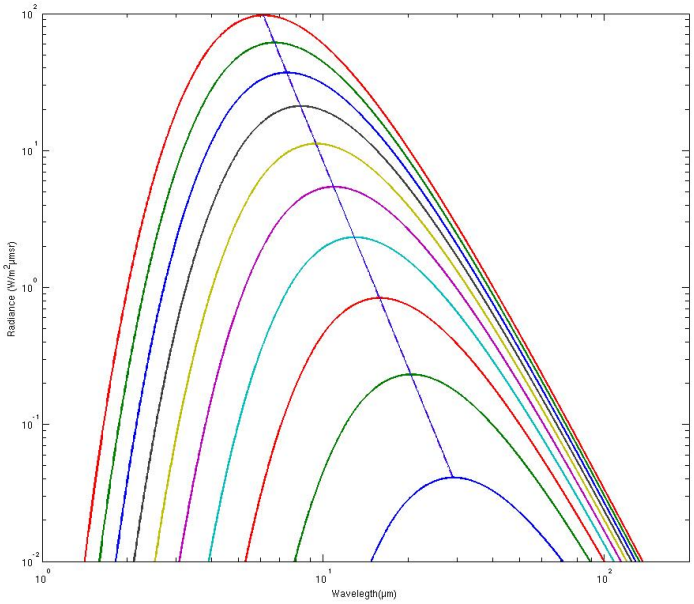

Figure 2.1: Planck's Distributions and Wien's Law

Performing integration of the Planck Distribution over all the wavelength interval we can obtain the total emitted power of a Black Body only as a function of temperature and the *Boltzmann's Constant*($\sigma = 5.6710^{-8}\frac{W}{m^2K^4}$)

$$E_b(\frac{W}{m^2}) = \sigma T^4 \tag{2.3}$$

But of course in reality, perfect black bodies never exist. This is why a dimensionless parameter known as **emissivity** is defined, in order to classify real materials in relation to a black body at the same temperature as the real body. Therefore in general, emissivity is a spectral property dependant on the temperature of the material:

$$\varepsilon_\lambda = \frac{E(\lambda,T)}{E_b(\lambda,T)} \tag{2.4}$$

This parameter helps us define the emissive power of a body with constant emissivity, also known as **Gray Bodies** :

$$E_b(\frac{W}{m^2}) = \varepsilon\sigma T^4 \tag{2.5}$$

However, in reality no materials present constant emissivity and this value is dependent on the wavelength, temperature, and many times on the angle of incidence of radiation. In our case, surfaces investigated will all be coated with a painting that will let the surfaces behave as gray bodies with an emissivity factor of 0.973 (almost black body), constant for our range of study.

Attending to how materials interact with radiation, other three parameters related to emissivity are defined: **absorptivity** (α), **transmissivity** (τ) and **reflectivity** (ρ). Absorptivity gives the portion of incident radiation that is absorbed by the body. Transmissivity gives the portion of radiation that is transmitted by the surface, and reflectivity is the portion of incident radiation that is reflected by the surface. According to this definitions and making a simple radiation balance, the expression (2.6) should be satisfied:

$$\alpha + \tau + \rho = 1 \tag{2.6}$$

It is also important to take into account **Kirchoff's Law of Thermal Radiation** which yields that, at each wavelength absorption coefficient and emissivity have the same spectral value ($\alpha_\lambda = \varepsilon_\lambda$)

2.2 Conduction

Conduction is the type of heat transfer that takes place inside solids and fluids due to temperature gradients inside them. The heat flux that is transported by conduction is also dependent on a material property known as conductivity $k(\frac{W}{mK})$ which is a property of each material. The law that mathematically shows this is Fourier Law:

$$q''(\frac{W}{m^2}) = -k\nabla T \tag{2.7}$$

From this definition, using control volume theory for infinitely small volume the unsteady heat transfer equation for conduction can be obtained:

$$\frac{\partial T}{\partial t} - \alpha\nabla^2 T = q^* \tag{2.8}$$

In the last equation $q^*(\frac{W}{m^3})$ represents the internal generation of heat per unit of volume and α represents the thermal diffusivity of the material, which is defined like this:

$$\alpha(\frac{m^2}{s}) = \frac{k}{\rho c_p}$$

2.3 Convection

Convective heat transfer is a phenomenon that takes place in fluids due to their movement. This is usually the dominant form of heat transfer between solids and fluids and in fluids. Convection is dependent of many variables as it has a very big relation with the fluid flow. In our experiments we are interested in measuring the heat transfer between a surface and the fluid surrounding it. To approach a quantitative analysis of convection *Newton's Law* is used:

$$q''_{cv}(\frac{W}{m^2}) = h(T_{surface} - T_\infty) \tag{2.9}$$

$h(\frac{W}{m^2K})$, also known as heat transfer coefficient (HTC) is a very difficult value to obtain analytically as it is dependent on the fluid flow and certain properties of the surface. Normally, its value is obtained through empirical correlations of dimensionless numbers, such as $Reynolds(Re = \frac{\rho v D}{\mu})$ or $Prandtl(Pr = \frac{c_p \mu}{k})$, very used in Fluid Dynamics. The dimensionless number associated with h is the **Nusselt Number** ($Nu = \frac{hL}{k_{fluid}}$). As an example, in a forced convection case $Nu = f(Re,Pr)$.

It is important to note that T_∞ is the temperature of the fluid far away enough from the surface to that the temperature distribution can be considered constant (out of the thermal boundary layer)

2.4 Optical Properties of Materials

Intimately related with some radiative properties of materials are some optical properties that influence values such as transmittance, which is the main object of study in the first part of this paper. The most important optical property related to the transmittance is the **Refractive Index**, which is a dimensionless parameter that describes how any radiation propagates through that medium.

Theoretically, is defined as: $n = \frac{c}{v}$ where c represents the speed of light in vacuum and v represents the speed of light in the substance being treated. This parameter defines how radiation is bent when entering a material. This is described primarily by *Snell's Law*:

$$n_1 sin(\theta_1) = n_2 sin(\theta_2) \tag{2.10}$$

After this definition, it is expected that, in order to have a high value of transmittance, low values of refractive index would be desired in order to get the fewest losses of energy in the material.

Another important relation of transparent materials is the one between the transmittance and the length of the path covered by the radiation in the material.

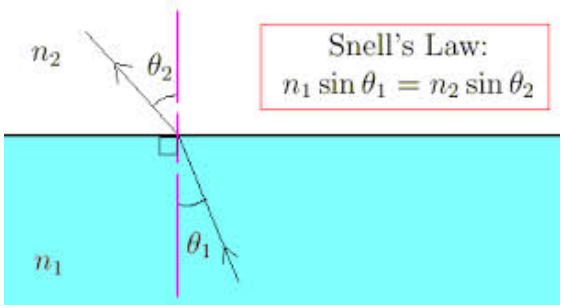

Figure 2.2: Snell's Law sketch

This is explained by $Beer - Lambert\ Law$. According to this law, the absorption of spectral radiation in a semitransparent medium is function of the absorption coefficient $k_\lambda(1/m)$ and the width L of the material transferring the radiation. If a monochromatic beam of radiation I_0 goes into a medium, the intensity of the radiation gets reduced due to the absorption following the law (2.11)

$$\frac{dI_\lambda}{I_\lambda} = -k_\lambda dx \tag{2.11}$$

Integrating equation (2.11) from 0 to L we can obtain a relation between the radiation transferred through the material as a function of the width of the semi-transparent medium, which results in the exponential decay known as $Beer's\ Law$, which can be used to infer the spectral transmittance of the medium:

$$\tau_\lambda = e^{-k_\lambda L} \tag{2.12}$$

In the first part of the investigation carried on in this work we have tried to adjust experimental values of temperature taken with an IR camera to a law of this kind basing on certain hypothesis described after.

Chapter 3

Literature research for IR transparent window

The measurement technique used in this project for obtaining temperature distributions over surfaces has been IR thermography. The main advantage that this method provides is that it is a non-intrusive method as it is able to measure the regions of interest without disturbing the results. It also helps us obtain an almost continuum distribution (always taking into account that the camera measures temperature for discrete points) compared to other methods such as thermocouple mapping, in which interpolation in order to obtain a continuum distribution is less exact. Also, the camera that will be used can provide a very low uncertainty (0.01^oC). On the other hand, IR thermography is very sensible to radiative properties of the components being analysed and deep knowledge of their spectral behavior must be known. The main two radiative properties that this paper will be focusing are emissivity and transmittance of the material that will be used. This is due to the fact that our IR camera will work optimally when analysing surfaces with high emissivity and with high transmittance for the medium that are put between the camera and the regions of interest we are investigating. In fact the first part of the study developed has been to check some properties of different materials in order to assemble a special window between our camera and the surfaces we are interested in.

After doing some literature research it has been found out that there are a few typical materials that are highly transparent to IR radiation and therefore adequate to be used as a window between our termographic device and the surfaces which temperature we want to measure.

By the knowledge accomplished during this investigation, the most used materials for this purpose are the ones analysed below. The final decision must be made taking into account the wavelength interval in which our camera works. Also a low value of the absorption coefficient should be good for our purposes apart from

other secondary characteristics such as mechanical and thermal properties. As a reminder, the filtered spectral response of our IR Camera is at the interval $3-5\mu m$. The most commonly used materials and their characteristics are the following:

Calcium Fluoride (CaF_2):

CaF_2 is useful when working in non agressive thermal ambient, due to its poor thermal behaviour. However, the conditions in our lab do not usually get very extreme, and therefore CaF_2 can have enough thermal and mechanical properties for our experimental purposes. When regarding its optical response, it is normally considered that CaF_2 has quite good transmission rate (over 90 per cent) between $0.25 - 6\mu m$ which would accomplish our objective. We have to take into account also the reflectiveness of this material, which is sometimes improved thanks to special coatings available in the market.

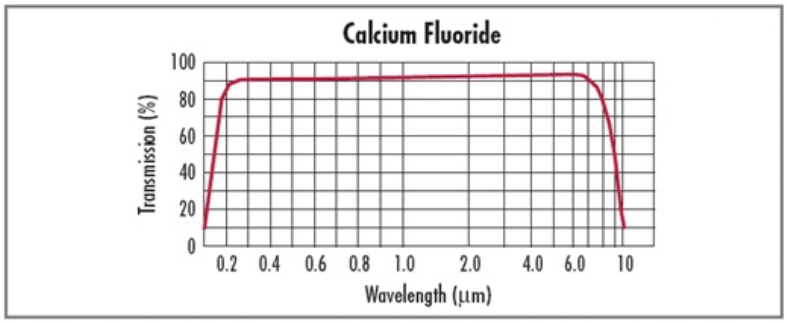

Figure 3.1: Spectral Transmittance of Calcium Fluoride

Barium Fluoride (BaF_2):

BaF_2 has more than 90 per cent of transmittance for wavelength from $150nm$ to $8\mu m$, which also makes it useful for IR thermography. However, it has less resistance to water than CaF_2, but enough for the purposes we have in our lab. Also, BaF_2 has a low index of refraction which allows us to use it without any special anti reflecting coating. In general the decision between this and CaF_2 can be made basing it in the price due to the good expected performance of both materials for our lab.

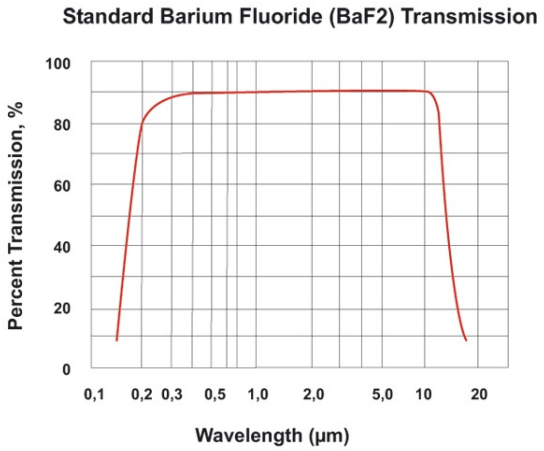

Figure 3.2: Spectral Transmittance of Barium Fluoride

Sapphire (Al_2O_3):

Sapphire has also a wide range of applications and is has a wide use in the industry for similar cases as the one we are trying to work with. Theoretically, Sapphire acts as a transparent material for MWIR so it was supposed to fulfil the requirements we need (transparent material between $3 - 5\mu m$ as it can be seen in the graph below. However, this material has already been tested in an experimental rig assembled in our laboratory, and the results showed that this material wasn't capable of transmitting all the IR radiation, and that had a high value of specular reflectiveness, so this material will be discarded beforehand. The bad results presented by this material can be checked easily at any moment as there are sapphire windows in our lab.

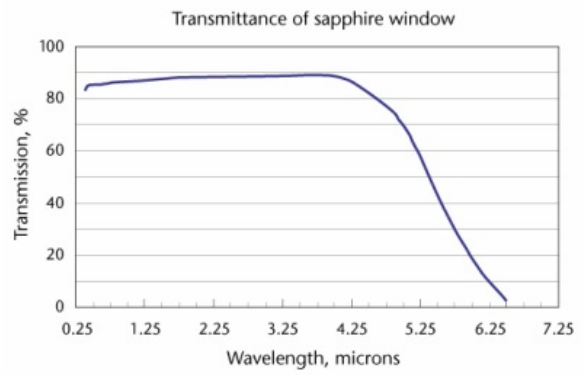

Figure 3.3: Spectral Transmittance of Sapphire

It can be found that the transmittance of this material falls dramatically from $4 - 5\mu m$ which obviously makes this material not appropriate for our objectives.

Zinc Selenide ($ZnSe$):

Zinc Selenide is usually the best choice when working with long wave IR radiation, as it keeps a high value in transmittance from $3 - 12\mu m$. Nevertheless, this wide spectral response from $ZnSe$ makes this material more appropriate for other applications than for the one being attempted in this work. Usually, this material is the first choice for high power Laser systems due to its good absorption parameters (low absorption coefficient) and its good properties against thermal shock. Also it is good to bear in mind that high transmittance of this material starts at $3\mu m$, which is our lower limit, therefore we should make our decision trying to choose a material in which our interval of work is fully inside the interval of high transmittance. It is although possible to find ZnSe windows with special anti reflecting coatings that make the window transparent from $0.6 - 12\mu m$

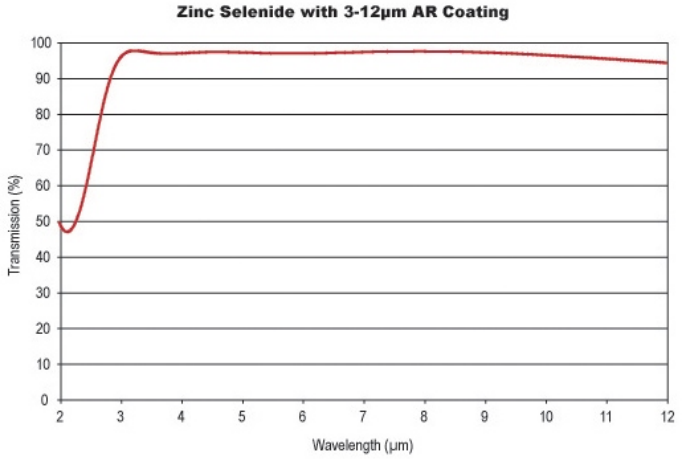

Figure 3.4: Spectral Transmittance of ZnSe

Germanium (Ge):

Germanium can also be a good choice as it presents good optical properties, such as a low index of refraction, and a quite good transmittance for a wide range of wavelength. Usually, Germanium for optical applications must be used with an anti reflecting coating, as without it, this material has a big reflectivity value. With this coating Germanium properties are similar to $ZnSe$ in terms of spectral transmittance. But again, the reasons for not choosing this material will be similar as the ones said when presenting the possibility of $ZnSe$, as it is probably a more suitable choice

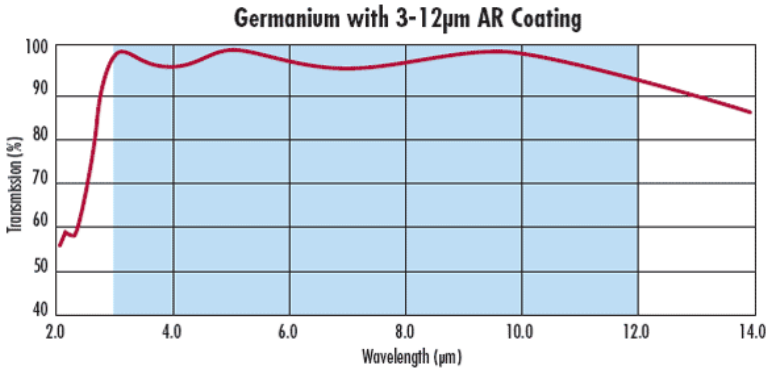

Figure 3.5: Spectral Transmittance of Barium Fluoride

Silicon Si :

Silicon windows for IR measurement techniques give usually good results for the interval $1.2 - 7\mu m$ and companies that sell optical products such as Edmund Optics have in their inventory silicon windows with especial anti reflection coating for $3 - 5\mu m$, which is the range in which our camera works. On the other hand, silicon is opaque in the visible spectrum which is a drawback as we would not be able to see across the window. However, this is a small drawback as our intention would be to place the window in a small part of a transparent plexiglass window. Finally, basing our decision on quality/economic factors, the material chosen was Silicon, and all the experimental investigation has been done about this material.

Chapter 4

Experimental Investigation of Silicon Window

The first experimental study carried out in this work was the analysis of the behaviour that a $\phi 50mm$ silicon (Si) window when interacting with our IR camera in the measurement of the temperature distribution over surfaces. In this section the details of the experimental set-up is explained.

4.1 MWIR Transparent Silicon (Si) Window

The window used for the investigation is a $\phi 50mm$ is bought from Edmund Optics. The product has a especial coating for avoiding bad reflections in the range $3-5\mu m$. This window has a thickness of $3mm$ The supplier provides the following spectral transmittance:

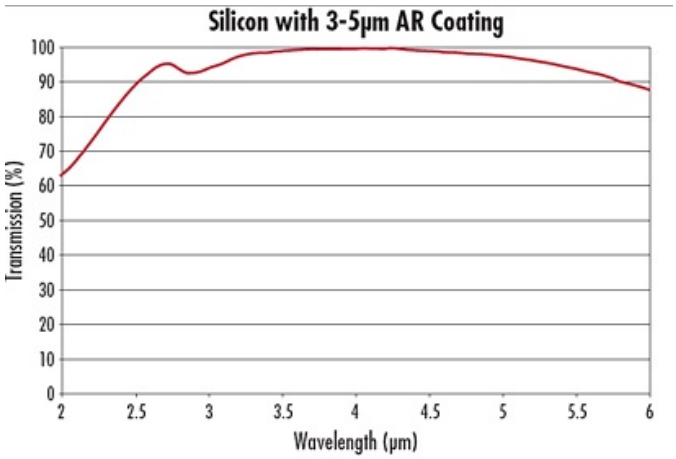

Figure 4.1: Spectral Transmittance given by Edmund Optics

4.2 Transmittance Calculation and Uncertainty

In order to obtain numerical values for the transmittance of the silicon windows, we will be using our IR-camera, which output will be counts, and after the conversion explained, temperature. Therefore, basing on the theoretical fundamentals already explained we need to establish a mathematical relation between the measured temperatures and the transmittance of the medium in between. Also, the uncertainty of this expression will be computed.

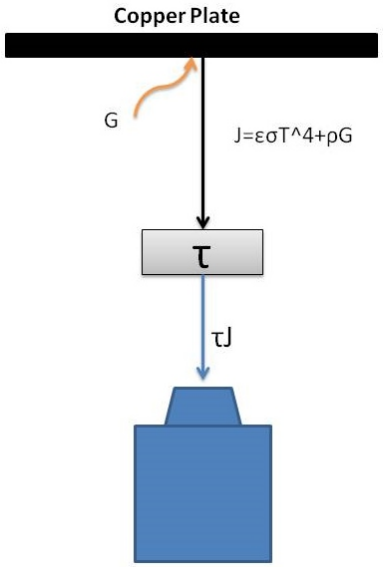

Figure 4.2: Transmittance Calculation Sketch

The idea is that we compare what the camera measures with and without the Silicon window in between. What the camera measures originally is directly related to the radiosity (J) of the surface. If we call T_w to the measurement with the window in between and T_{nw} to the measurement without window:

According to the sketch above and calling $G = \sigma T_\infty^4$ to the irradiation from the surroundings to the surface:

$$\tau = \frac{J_w}{J_{nw}} = \frac{\varepsilon\sigma T_w^4 + \rho\sigma T_\infty^4}{\varepsilon\sigma T_{nw}^4 + \rho\sigma T_{\infty,nw}^4} \tag{4.1}$$

If we assume that the reflectivity of the surfaces is very small then we approximate the expression of the transmittance to:

$$\tau = (\frac{T_w}{T_{nw}})^4 \tag{4.2}$$

Since both of the measurements with and without window have a certain uncertainty, an uncertainty will be added to the transmittance calculated by using the total differential of the defined function:

$$\delta\tau = |\frac{\partial\tau}{\partial T_{nw}}|\delta T_{nw} + |\frac{\partial\tau}{\partial T_w}|\delta T_w \tag{4.3}$$

Knowing the camera accuracy; $\delta T_w = \delta T_{nw} = \delta T = 0.01K$ and that the temperature in K has always a positive value, we get the analytical expression for the propagated uncertainty of using expression (4.4):

$$\delta\tau = 4\frac{T_w^3}{T_{nw}^4}(1 + \frac{T_w}{T_{nw}})\delta T \tag{4.4}$$

According to the expression we defined for τ we can obtain a more compact expression for the added uncertainty:

$$\delta\tau = 4\tau^{0.75}(1 + \tau^{0.25})\frac{\delta T}{T_{nw}} \tag{4.5}$$

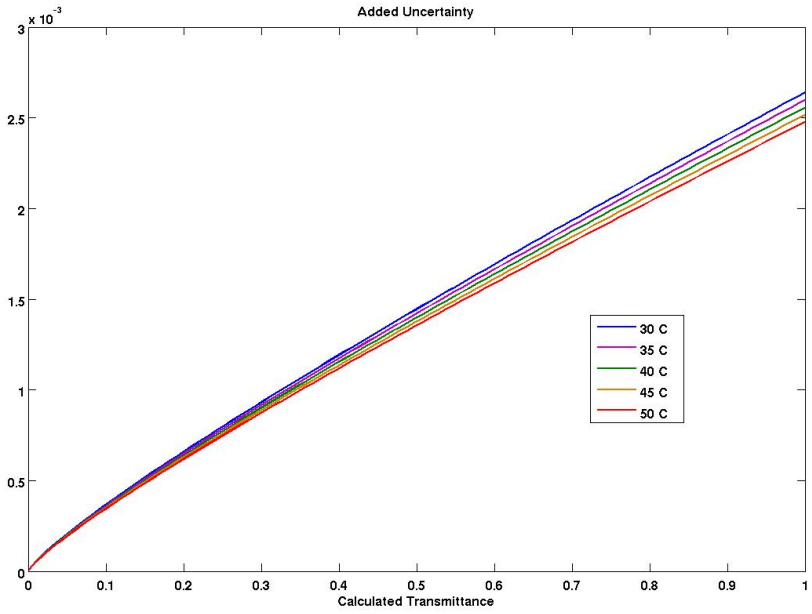

Figure 4.3: Added Uncertainty for five Absolute Temperatures (T_{nw})

As it can be seen on the previous figure, the value of the added uncertainty is very small to the already existing uncertainty in the measured value of temperature.

4.3 IR Transparent Window Implementation

For the experiment, there was also need to design a way to put our Silicon window in the linear cascase for the camera to have vision of the instrumented vane through it. To do this, an already existing glass window was used. This old glass window has machined two small rectangular windows (see Fig. 4.3) on it. One of them is removed and will be manufactured in a workshop to let the Silicon Window be introduced in it as it is shown in the exploded view.

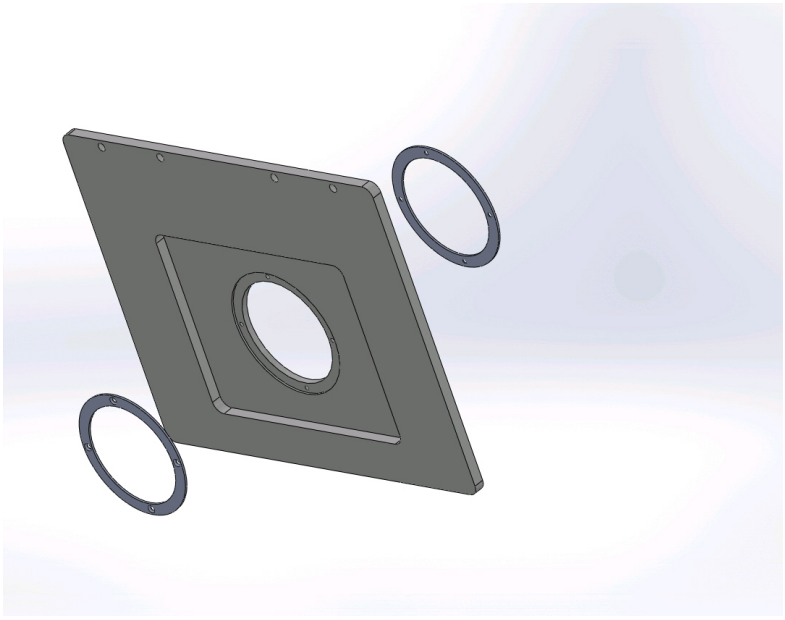

Figure 4.4: Si Window Implementation

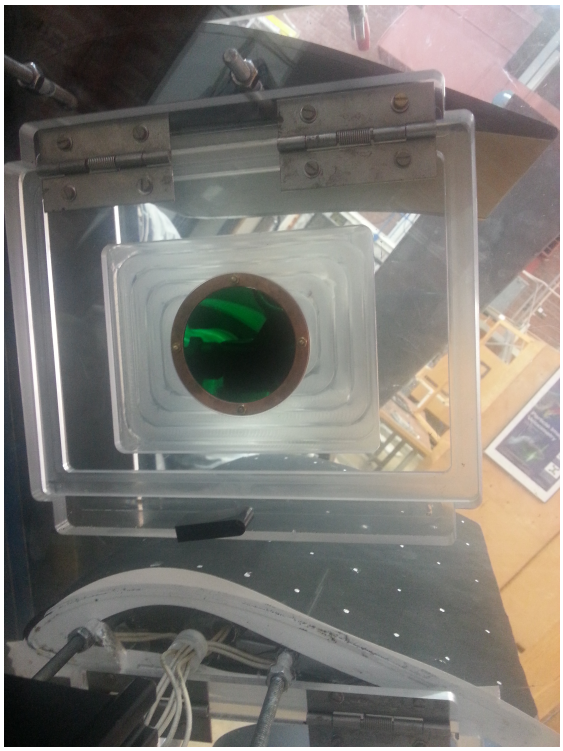

Figure 4.5: Silicon window in the linear cascade

As it can be seen, the Silicon window will be held by two thin metal rings screwed to the rectangular window. With all this everything is ready to take thermal images of the vane in the linear cascade in the interest point.

4.4 Window Results

In this section we show what temperature distribution we can measure with the window in between. The following images show the temperature measured with the window in between. In figure 4.6, the temperature difference between the cases with and without window in a radial line is plotted.

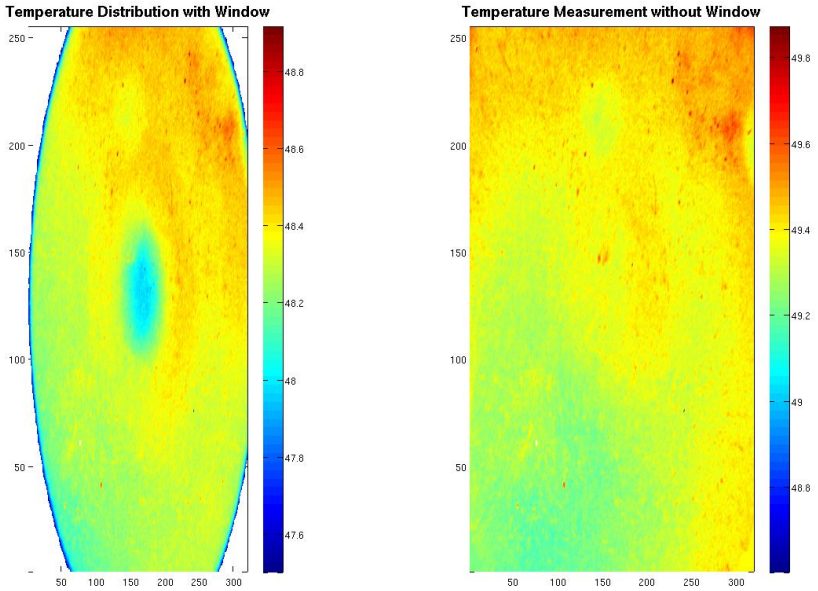

Figure 4.6: Same Surface with and without window in between

As it can be seen from figure 4.6, some specular reflection appears on the middle of the window. In principle this could be a problem to implement the window in future experiments, especially because our desire would be to obtain an uniform distribution through the window in order to apply the same correction to all the pixels of the images we take.

However as it will be explained more deeply later, placing the window with a relative angle the specular reflection will move from the image and we will be able to get an uniform temperature.

Below, the temperature difference between the cases with and without window in a radial line is plotted. The difference showed is quite constant excluding the specular reflection that occurs in the middle:

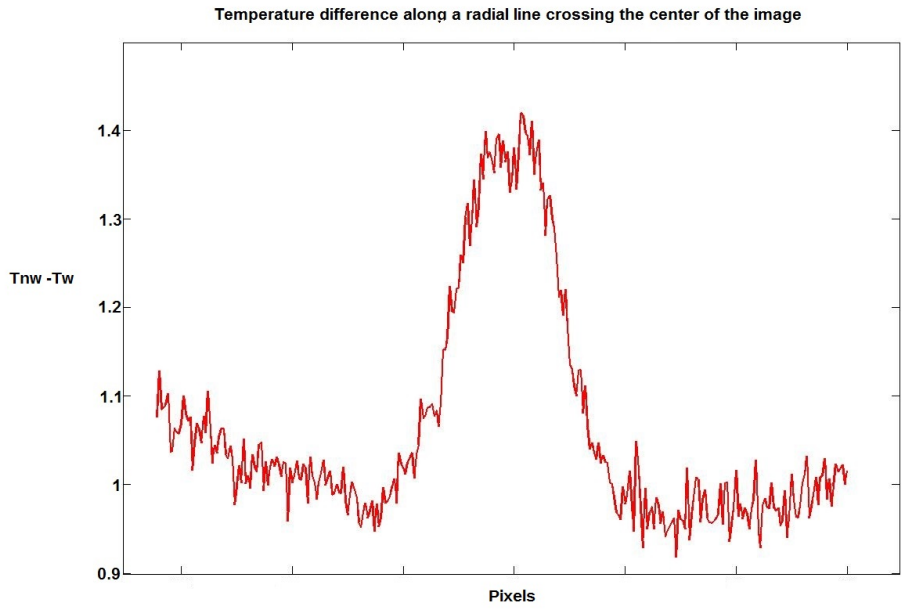

Figure 4.7: Difference distirbution along a radial line of the image

4.4.1 Angle and Temperature Dependence

In order to investigate the transmission decay of the window with the relative angle, the calibration device has been used. Angles up to 45^o for different temperatures have been studied. The following two figures show the same plots with different axis scale. The first one wants to show especially how the specular reflection zone moves from the center as the relative angle increases. Of course, the position of the reflection zone is fully dependent on the distance between the objective and the surface and therefore the limit angle from which the reflection moves out will not be constant for all relative dispositions.

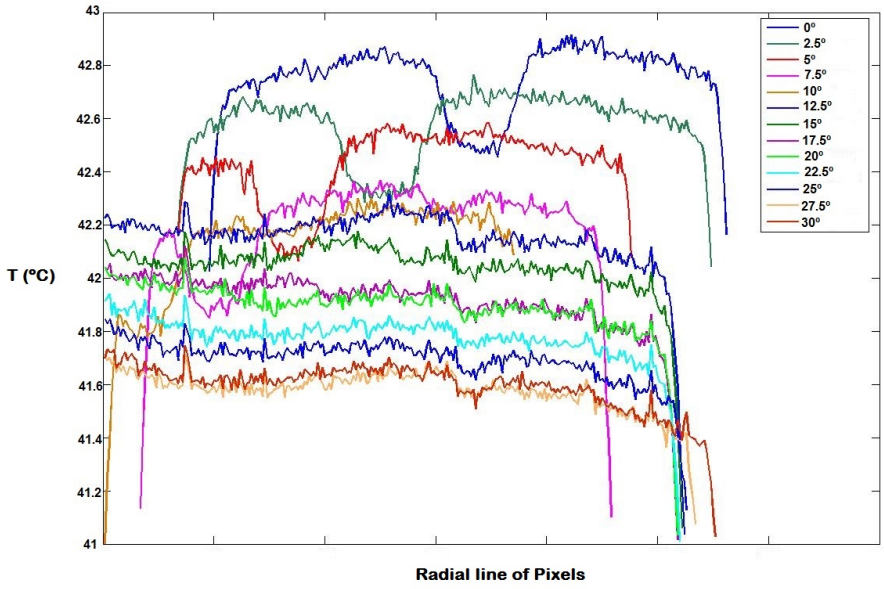

Figure 4.8: Temperature decay with relative angle

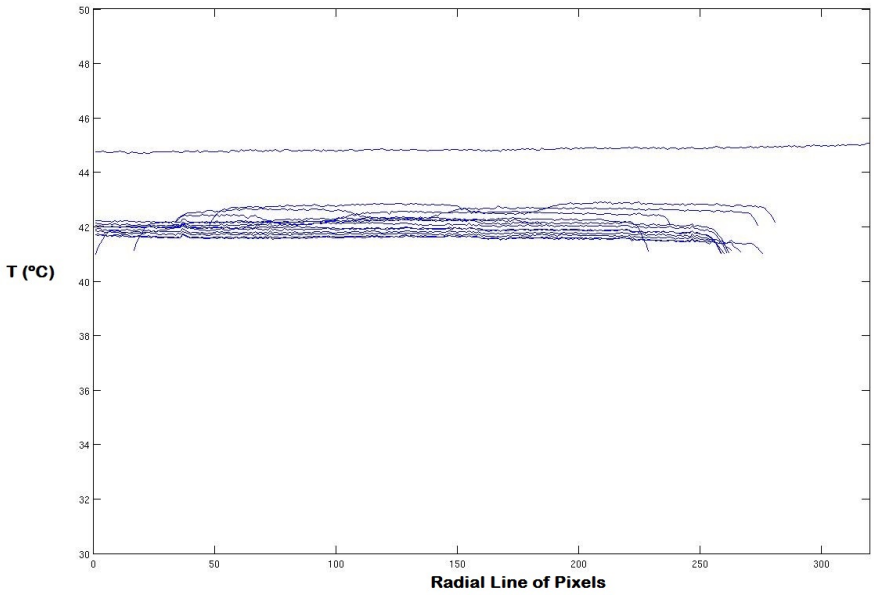

Figure 4.9: Same plot as before with bigger scale. It has also been included a line of the measurement without Si window in between)

In Fig. 4.8 we can see how the limit angle for this case is 10^o and that for a relative angle bigger than this the temperature distribution seen through the window is mostly uniform.

Knowing this we have tried to match the temperature decay with the *Beer − Lambert Law* explained in the theoretical background section, assuming that if the angle increases, so does the path of radiation in the semi transparent medium. This fact must be obviously true, but the transmittance values calculated with the expression explained did not match as they would be expected just regarding the *Beer − Lambert Law* and using a geometrical relation between the radiation path and the angle, following this sketch:

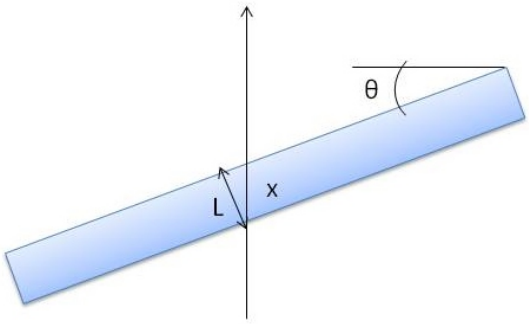

Figure 4.10: Sketch for transmittance calculation

According to fig. 4.10 $x = \frac{L}{\cos\theta}$ and using *Beer − Lambert Law*:

$$\tau = e^{-k_\lambda x}$$

$$\tau = e^{-\frac{k_\lambda L}{\cos\theta}} \tag{4.6}$$

In the following plot this expression has been represented for different absorption coefficients to then be compared with the experimental variation we obtain for $0 - 45^o$. From both images we can see how the decay is much higher in the experimental results. The discussion of this discrepancies is carried out afterwards.

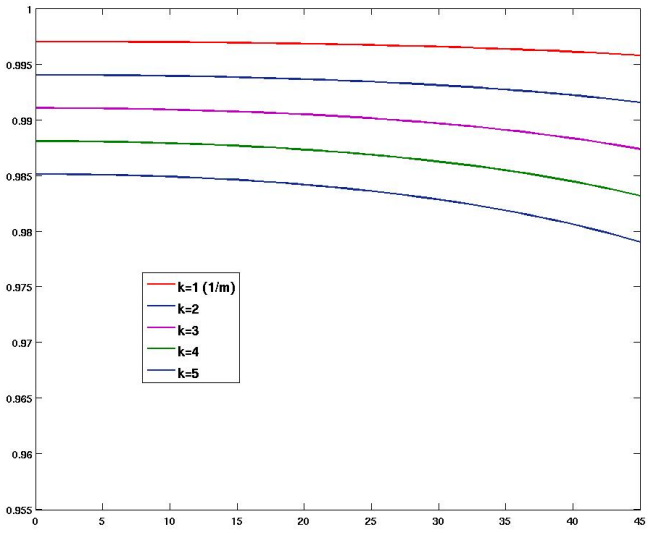

Figure 4.11: Theoretical Variation of the Transmittance with the relative angle for different k_λ values (Beer-Lambert Law)

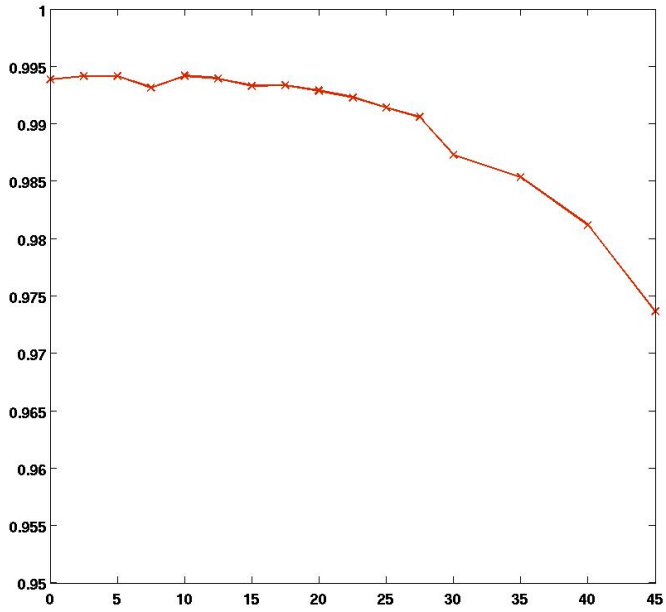

Figure 4.12: Experimental Variation of the Transmittance with the relative angle for the surface at 40^oC

The comparison between figures 4.11 and 4.12 show that for small angles the theory assumed fits well if we assume an approximated absorption coefficient of $k = 2m^{-1}$. However we see that for bigger angles this curve does not match at all with the experimental results. The main reason for this is probably that the $Beer - Lambert\ Law$ describes the transmission for **monochromatic** beam of radiation, and that the correction that relates the angle variation with the radiation path may not be totally true due mainly to the refraction inside the medium ($Snell's\ Law$).

The following study has focused on analysing whether the temperature variation produces a big variation in the measured values of transmittance or not in our work range $(30 - 45^oC)$.

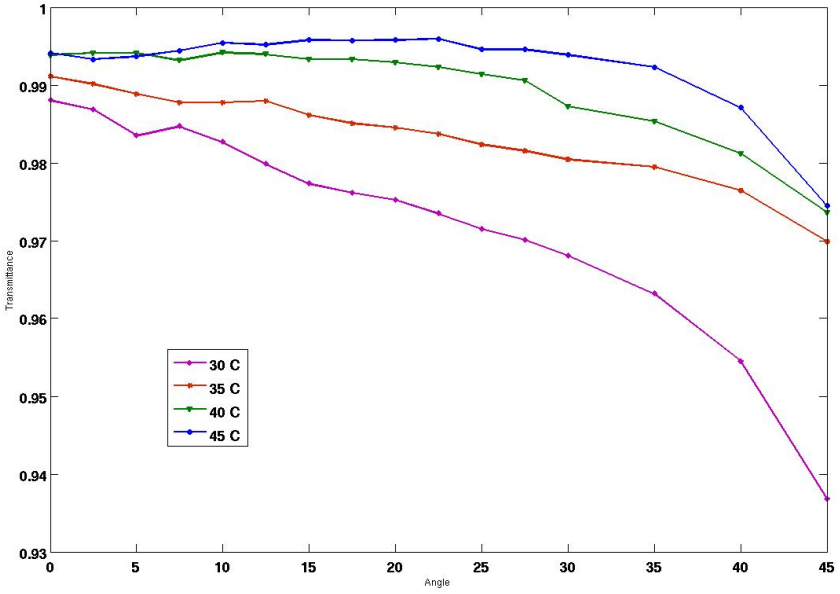

Figure 4.13: Experimental Variation of the Transmittance with the relative angle for the surface at five temperatures

As it can be seen the behaviour of the window is better for higher temperatures and the decay is less strong also. Now we will try to fit the transmittance to correlations that let us apply this law depending on the temperature of the target surface and the relative angle of the window. This correlations can then be used in a experiment in the linear cascade in our lab with the window. This will provide validation or not to this experiments with the transparent window.

Curve fitting has been done using CFTool in MatLab. The type of curves that best provide fitting of the transmittance dependence with the angle are exponential curves with two terms. Functions of this type

$$f(x) = ae^{bx} + ce^{dx}$$

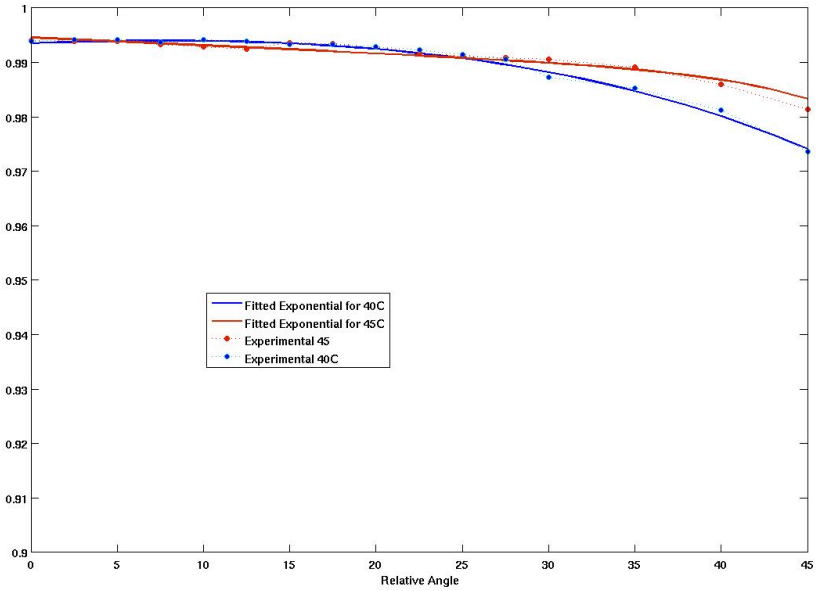

Figure 4.14: Experimental Results and their fitted curve for two different target temperatures

Experimental data for this case do not match exactly with the ones shown in Fig. 4.11 due to the fact that the data where acquired during different experiments

4.4.2 Si Window behaviour in the Linear Cascade facility

To know how would the implementation in our lab facilities we have used the semitransparent window in the linear cascade as it has been explained before. This analysis has been made on an endwall designed by Carlos Jimenez that was used before for some heat transfer experiments that helped understand the thermal behaviour of the endwall in the OGVs of an aeroengine.

To do this we put the Linear Cascade in an on-design condition and we have taken photos withour window and with the silicon in between. Afterwards, we have used the data of transmittance we had obtained during the investigation, and an polynomial function of absolute Temperature has been generated using CFTool in

MatLab for our temperature range and for the relative angle that the camera has been taking the image.

This polynomial is applied to the temperature measurement as follows:

$$T_{corrected} = \frac{T_w}{\tau(T)^{0.25}}$$

Finding a general function of the angle and the temperature at the same time was a very difficult task and that is why the best option would probably be to generate different polynomials function of temperature once we know the relative that our camera is using.

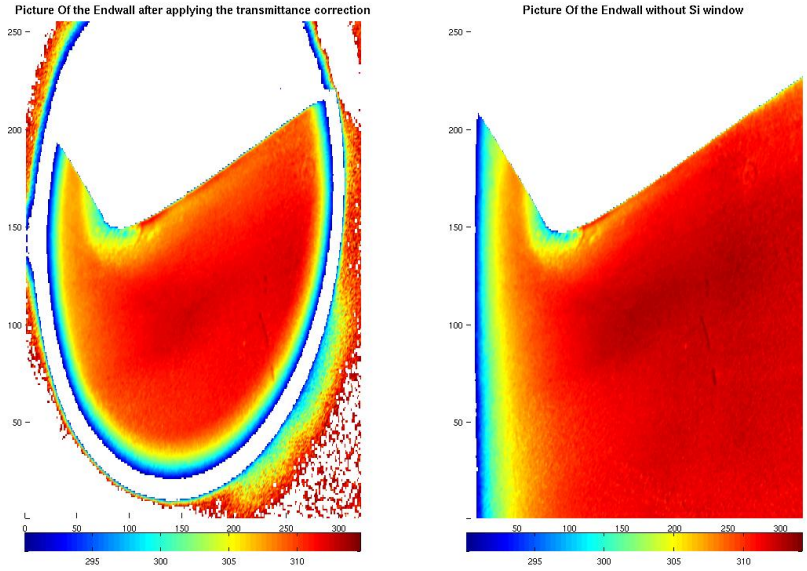

Figure 4.15: Leading edge region at the pressure side of the vane with and without window

Fig. 4.15 shows filtered image of the leading edge region at the pressure side of the vane close to the endwall. It can be seen how after the correction both images look practically identical.

Chapter 5

Camera Setup

In this section the corrections and improvements made during this work period on the camera setup are explained. Especially, the Non Uniformity Correction (**NUC**) that the camera pixels need has been studied thoroughly as well as the bad pixel correction in order to avoid using the software that the camera system provides and use a program designed in our department with LabView.

5.1 NUC. Theory and Implementation

The Non Uniformity Correction is a correction that needs to be applied to every detector in our camera so that for an uniform input, the output that the camera (every sensor output) gives is also uniform. In our work range, it is known that the camera sensors have a linear response. Therefore, doing a **two point NUC** must achieve of objectives. The two points will be two surfaces at different and uniform temperature. The specific temperature of each source is not of big importance as long as the lower temperature source is lower than the lowest temperature of interest, and that the higher temperature surface is far from saturation (around 75% level of the measurable dynamic range). In our case, the cold surface will be a black coated surface of aluminium at room's temperature, and the hot source will be the calibration surface at high enough temperature.

It is also of interest to say that performing an external NUC results of much more interest than using the internal sources that the camera system already has. This is because using external sources the camera optics are also taken into account.

In theory, multiple point NUC can be done without big problems and it would give more better results than a two point NUC.

Mathematics of NUC :

The idea of NUCs is to apply to each of the $ij-th$ photo-detectors a **gain** (a_{ij}) and an **offset** (b_{ij}). Then from the *Raw Pixels*, the corrected imaged is obtained:

$$Corrected = RawPixels * a_{ij} + b_{ij}$$

In a multiple point NUC with n points, the way to proceed is with the following matrix method, which is an application of the *Linear Least Square* for an over determined system such as $\mathbf{Xy} = \mathbf{b}$ The Least square solution in this kind of problem is computed as follows:

$$\mathbf{y} = (\mathbf{X}^T\mathbf{X})^{-1}\mathbf{X^T}\mathbf{by} = \mathbf{X}^+\mathbf{b} \tag{5.1}$$

Where $\mathbf{X}^+$ is the **pseudoinverse matrix** of $\mathbf{X}$. In our case the matrices $\mathbf{X}$, $\mathbf{y}$ and $\mathbf{b}$ are defined as follows:

$$\mathbf{X} = \begin{bmatrix} T_{ij}^{(1)} & 1 \\ \vdots & \vdots \\ T_{ij}^{(n)} & 1 \end{bmatrix}$$

-Where $T_{ij}^{(m)}$ is what the $ij-th$ photodetector measures in the $m-th$ point of the NUC.

$$\mathbf{y} = \begin{bmatrix} a_{ij} \\ b_{ij} \end{bmatrix}$$

-Which is the vector that contains the gain and offset that each photodetector requires. Finally, matrix $\mathbf{b}$ is defined for this problem like this:

$$\mathbf{b} = \begin{bmatrix} T_{mean}^{(1)} \\ \vdots \\ T_{mean}^{(n)} \end{bmatrix}$$

Where $T_{mean}^{(m)}$ represents the mean value of the measurement at each point of the NUC.

To sum up, we can say that in order to perform a multiple point NUC we have to solve a linear system as many times as photo-detector our system has using the Least Square Method, and after this we can assemble a matrix of gain (a_{ij}) and offset (b_{ij}) for each pixel. This algorithm has been performed using MatLab and the results of Gain and offset for our two-point NUC (i.e. $n = 2$) will be shown after the Bad Pixel correction is explained.

5.2 Bad Pixel Correction

It is very common in imaging systems that some photo-detectors give output values totally out of range of the normal expected measurement. This is something that has to be corrected along with the NUC in order to obtain a good post-processed thermal image. This is studied applying statistics to the output that the camera gives for one of the uniform source used for the NUC.

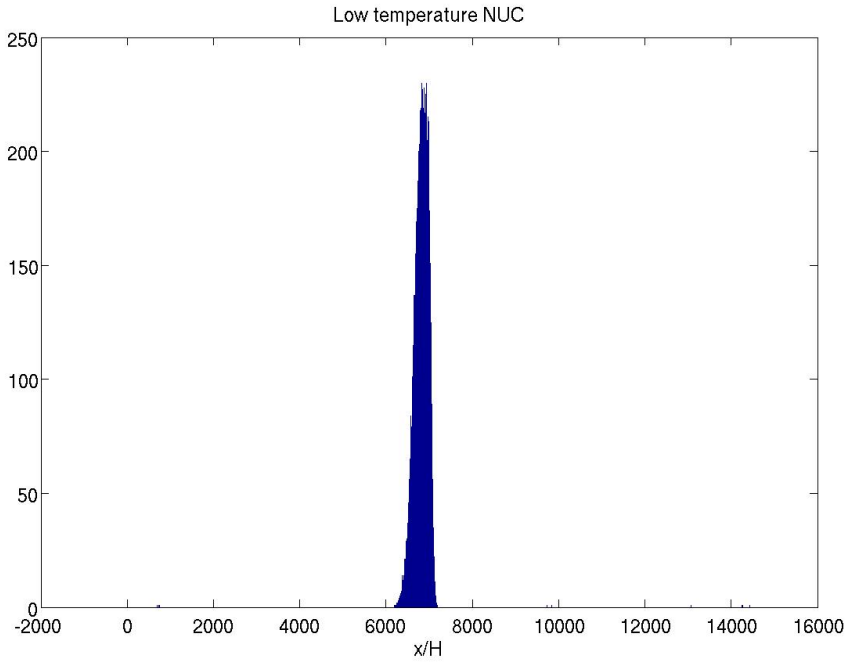

Figure 5.1: Histogram of count measurement by each photo-detector for the cold source of the NUC

In the histogram 5.1 we can see that there are few pixels that measure completely off the expected range of measurements. These photo-detectors are always the same ones and their location in the image can be easily known. To define the confidence interval for the measurements, we must work with the mean and the standard deviation assuming the histogram adjusts to a normal distribution, we define the maximum distance to the mean measurement relative to the standard deviation (σ). With this analysis, the location of the pixels that are out of our confidence interval will be known.

A lineal interpolation is made to this pixels with their surrounding ones and this is applied also to the gain and offset coefficients. After This, we have the matrix of gain and offset fully defined and ready to be applied to the raw image.

In the following figures, we show the bad pixel locations, the gain and offset distribution, and an image before and after the NUC and BP correction:

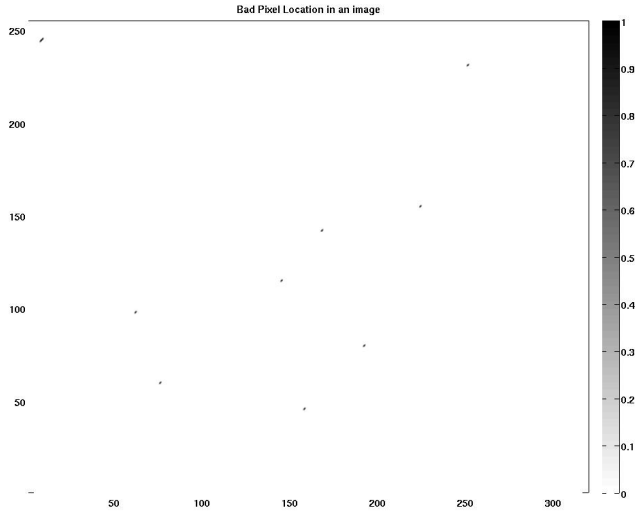

Figure 5.2: Location of the Bad Pixels in the Image

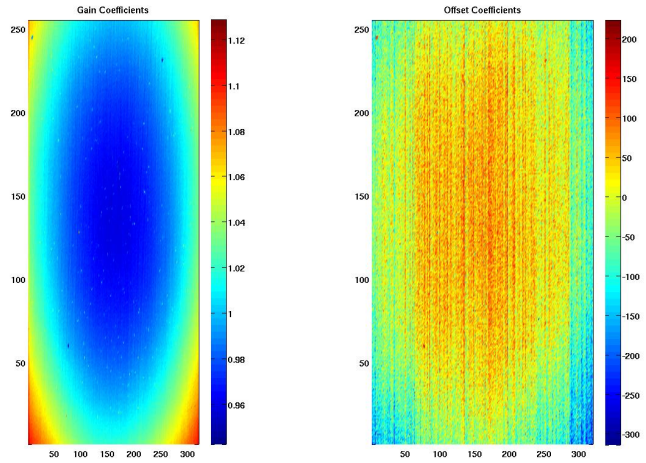

Figure 5.3: Gain and Offset coefficients

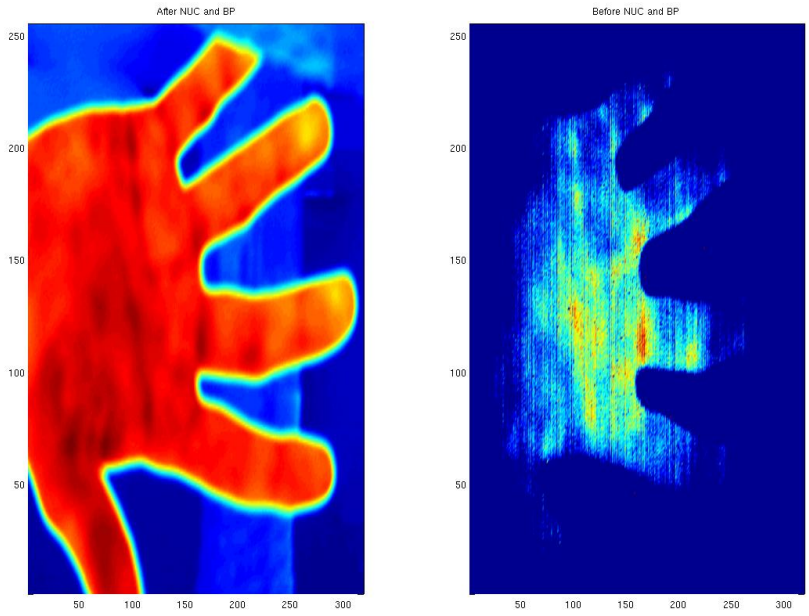

Figure 5.4: Image before and after applying the corrections

5.3 Camera Calibration

The last step in the camera setup for our experiments is to calibrate the camera in order to transform the measurement by the photo-detector (counts) into temperature. This is done using the software RCal by FLIR Systems which calculates polynomial equations that can be used to convert counts to radiance values and then from these ones to temperature. The software recommends us to adjust from counts to radiance and from radiance to temperature polynomials of 4^{th} grade. Therefore we will need 5 points measured in order to get the five coefficients of the two polynomial needed, this is done with the calibration tool used for the Silicon window study set at five different temperatures (the election of this temperatures has to be based in the work range of our experiments obviously). The theoretical radiance is calculated by the software using Planck's Equation in the wavelength interval that the camera works.

Chapter 6

Heat Transfer Experiment Setup And Facility

This part of the report shows a heat transfer experiment made in a linear cascade rig located in Chalmers University of Techngology. This experiment has then to be compared to previous results in experiments already carried on in our division. Our aim will be to obtain HTC in the surface of an OGV.

6.1 Linear Cascade Rig

Chalmers' Applied Mechanics Department has a subsonic linear cascade which aim is mainly to validate numerical methods to compute flow fields (CFD), and to improve our knowledge of the flow field around the outlet guide vanes (OGV) in jet engines. The test section is composed by two parallel discs where the inner discs constitute the upper and lower endwalls of the OGVs of the jet engine. In the test section there are located four OGVs and the pitch between them is 240 mm. One of these vanes will be especially instrumented for our heat transfer measurements, while the other three are made of plastic material and help to control the periodicity of the flow.

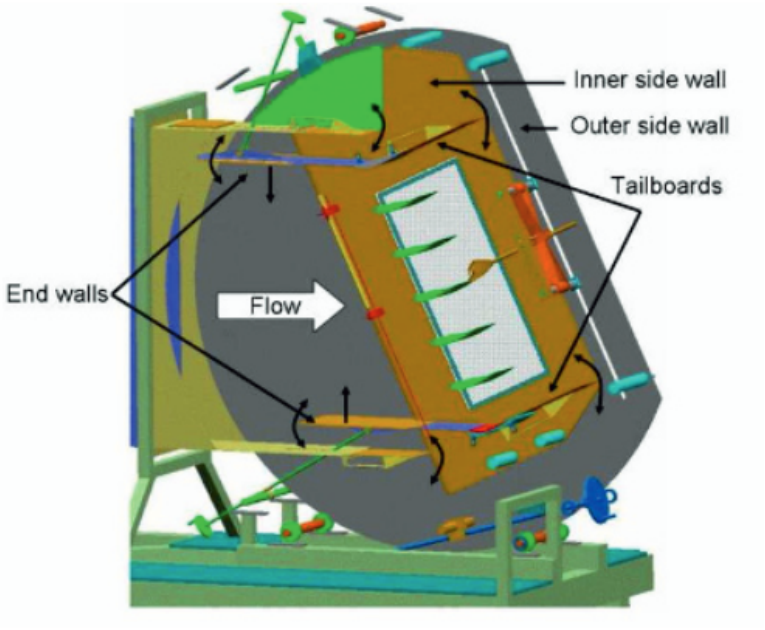

Figure 6.1: Linear Cascade Test Section

The linear cascade let us study different operation points (air velocity and angle of attack) of the OGVs. In our case, the study is focused in two off-design points (angle -25^o and -40^o) and the on-design point (25^o)

6.2 The Instrumented Vane

The instrumented vane where the heat transfer measurements are done is designed by GKN Aerospace and was manufactured by a workshop. It has an aluminium core (desirable for its high thermal conductivity ($k = 210\frac{W}{mK}$). It also has three passing holes where three cylindrical heaters can be put. Over the aluminium core we put a layer of low conductivity material in order to create a big temperature gradient. The material chosen to cover the core was silicone rubber, glued carefully so that the appearance of air bubbles between the aluminium and the silicone is avoided. If these bubbles would appear, these areas would have a much higher heat resistance and therefore the heat transfer distribution measured will not be correct. Then the silicone rubber is given the surface treatment already explained with Nextel Velvet-Coating 811-21 from Mankiewicz Gebr. & Co. This painting is applied using a spray gun.

6.3 Vane Coordinate Markers

The vane also needs to be marked in order to identify in our thermal images the real coordinates of the surface. These points are extracted from the CAD design given by GKN. This is done marking the points with a silver marker, which emissivity is much lower than the black coating one, and therefore they can be easily identified in a thermal image. In the following figure the coordinate of the markers are shown.

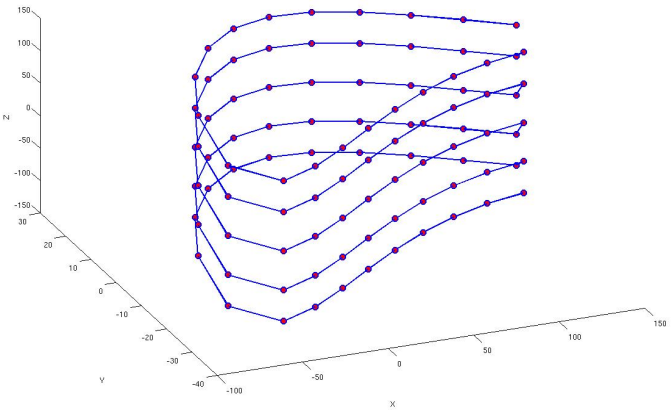

Figure 6.2: Vane coordinate markers

Figure 6.3: Instrumented vane with markers in the Linear Cascade

Chapter 7

Experimental Results

7.1 Image Post Processing

The thermal images once acquired are then post-processed using MatLab. The first step in post-processing is of course to transform the measurement in counts to temperature using the calibration polynomials. After, we have to interpolate the temperature measured in the silver marker zone. This is because, as the markers have very low emissivity, the temperature measured in these points is not the real temperature. The marker zones are selected manually from the image and are then interpolated with their neighbours that have a correct measurement.

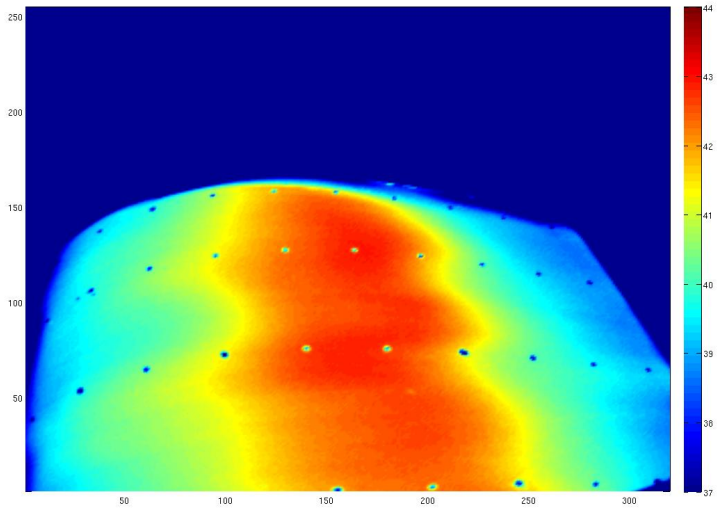

Figure 7.1: Suction Side 0-50 % span. In this figure it can be seen clearly how the markers give wrong values of temperature that need to be corrected:

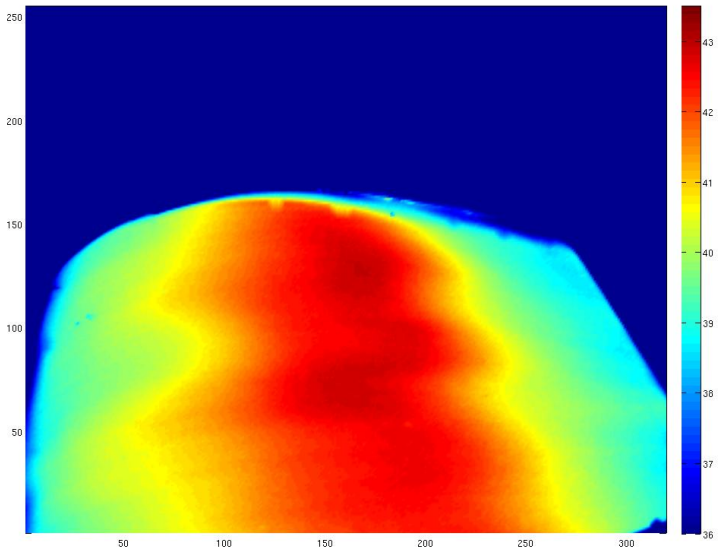

Figure 7.2: Suction Side 0-50 % span. after the markers have been interpolated and removed

The next step will be to assign the image coordinate (pixels) to the real geometry of the surface. This is done also manually over the image dividing it in rectangles that have in each of their four corners four markers which coordinates are known. With this a matrix can be assembled that contains the three coordinates and the temperature value at each point. This can then be exported after to fluent in order as a profile ANSYS FLUENT (.prof) file to use this temperature map as boundary condition for running our simulations to obtain the HTC distribution over the vane surface. In the picture below it is shown the exported temperature distribution on the suction side of the vane:

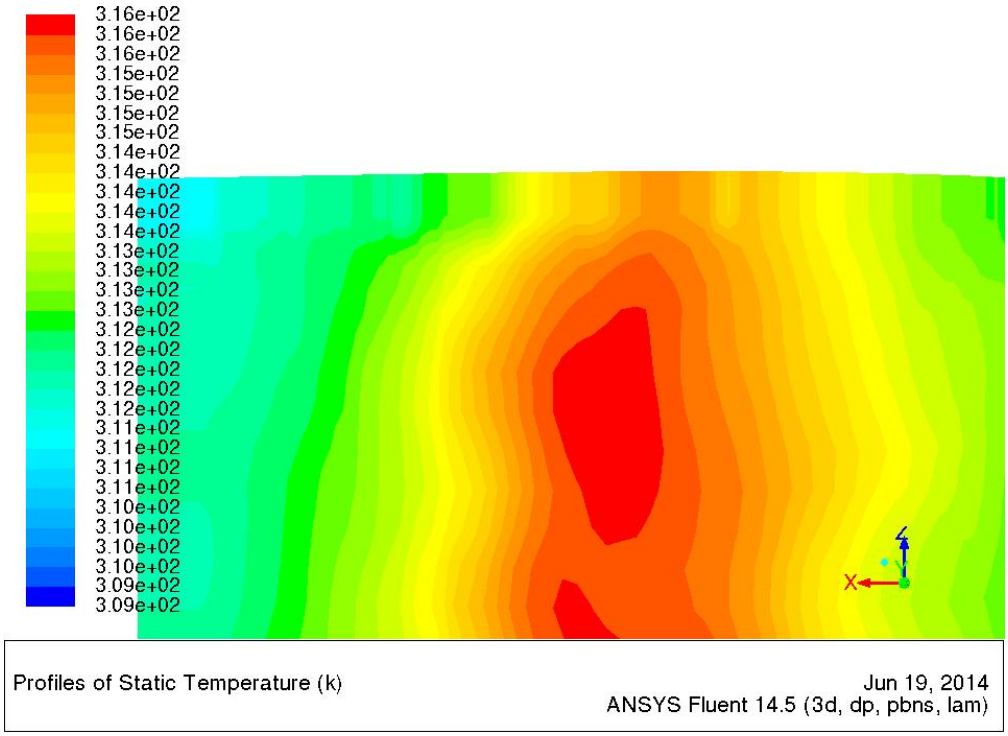

Figure 7.3: Suction Side 0-50 % span. after the map of temperature in this surface has been introduced to FLUENT

7.2 Fluent Simulations

ANSYS Fluent simulates the conduction phenomena that occur inside the vane. The mesh was developed and suplied by Borja Rojo using ICEM CFD and can be seen in the figure 7.4

Figure 7.4: Vane Mesh. The three cylinders inside are the three heaters

The program will use this mesh to solve in our case the conduction problem inside this body. The boundary conditions for this calculation will be the temperature of the heaters' surface (The one measured by a thermocouple placed inside one of the holes), and the temperature distribution in the silicone surface, which is the post-processed Temperature data of the image.

The solver uses Finite Volume Method **FVM** in order to obtain the distribution of heat flux in all the body. From these fluxes, the HTC can be computed and plotted easily in the surface of the vane for the cases the data was acquired

7.3 Cases

For this heat transfer experiment in the Linear Cascade, different cases have been studied, two off design cases and one on-design case. The on-design case is -25 º angle of attack, and off-design cases are -40 º and 25 º. It can be seen how changing the angle of the Outlet Guide Vanes produces important differences on the heat transfer along the vane. Also it would be interesting to investigate what is the difference between the 3D model used by FLUENT and the HTC values obtained using 1D approximation in matlab.

1D Approximation :

The 1D approximation simply assumes that the temperature in the aluminium is totally constant and that the gradient in the silicone layer can be assumed constant (as in 1D wall conduction case with no heat generation):

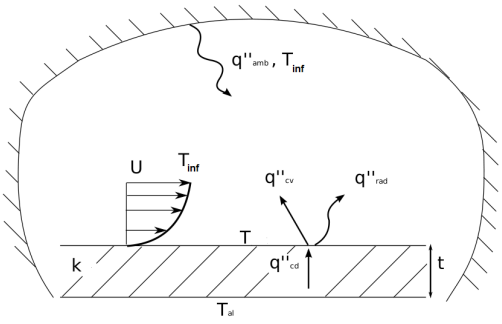

$$q"_{cd} = \frac{k}{t}(T_{al} - T_{inf}) \tag{7.1}$$

$$q"_{cv} = HTC(T - T_{inf}) \tag{7.2}$$

$$q"_{rad} = \sigma(T^4 - T_{inf}^4) \tag{7.3}$$

Knowing that $q"_{cd} = q"_{cv} + q"_{rad}$ we can compute HTC as follows:

$$HTC = \frac{q"_{cd} - q"_{rad}}{T - T_{inf}} \tag{7.4}$$

Performing a quick calculation using MatLab we see that the difference between the 1D model and the simulation is as big as 25% at some points,

7.3.1 Off-Design: 25 º air inlet velocity: 23 $\frac{m}{s}$

In the figure 7.5 we can see the HTC distribution in the surface of the suction side of the vane for 0-50 % span obtained from the heat flux distribution obtained by fluent. The pressure side for this case has not been investigated but it will be seen how the pressure side has a very uniform HTC in all cases. In the image 7.5, the transition zone can be seen very clearly.

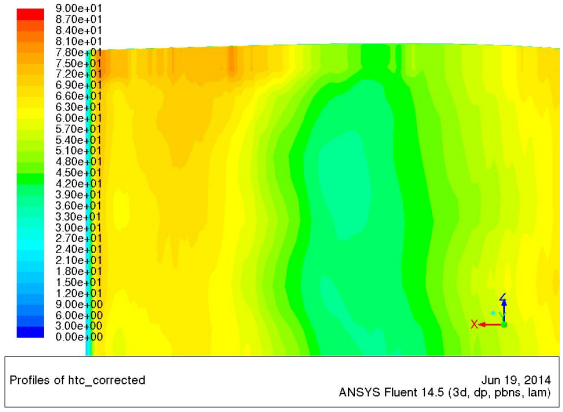

Figure 7.5: Plotted HTC on the suction side after including radiation losses to the ambient

7.3.2 Off-Design: -40 º air inlet velocity: 23$\frac{m}{s}$

In the figure 7.11 we can see the distribution of the HTC in the surfaces (both pressure and suction) of the instrumented vane. In this case the results of the calculations have been exported to CFX for post-process. The images were taken for 0-50 % span, but these have been doubled symmetrically as we assume the problem is symmetric. We can see how some complex structures appear and how there is also a clear transition zone.

a) 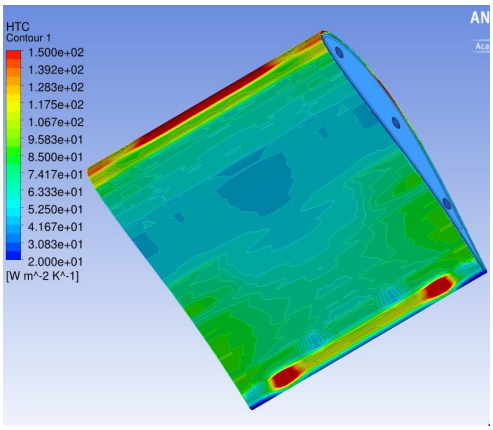

b) 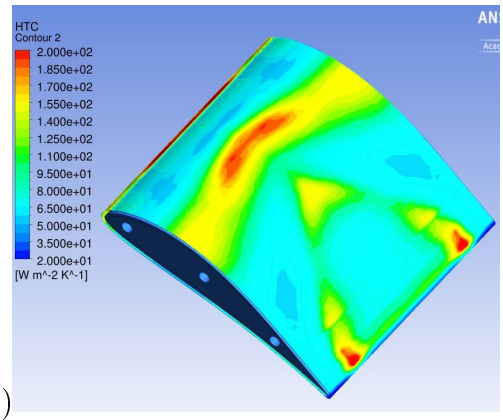

Figure 7.6: a) Pressure Side results b)Suction side results

7.3.3 Off-Design: -40 º air inlet velocity: 30 $\frac{m}{s}$

If the vane is investigated with the linear cascade working at 150 % regime the distribution of the HTC almost don't change in shape but only in the magnitude of the values compared to the 100 % case.

a) 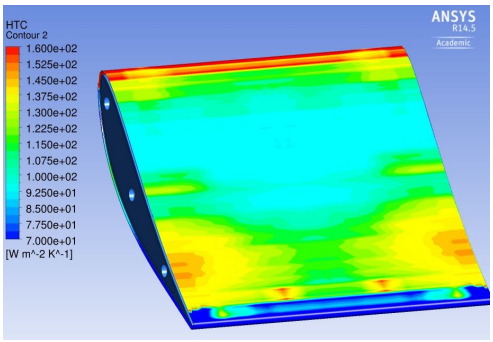

b) 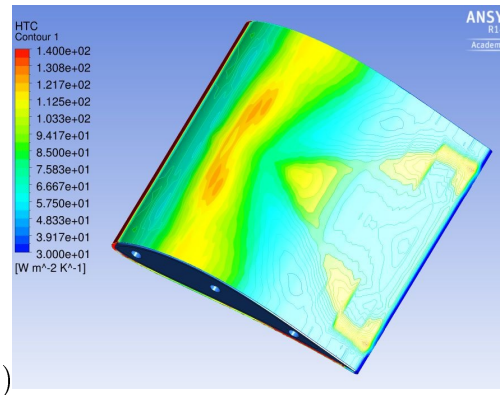

Figure 7.7: a) Pressure Side results b)Suction side results

7.3.4 On-Design: -25 º air inlet velocity 20 $\frac{m}{s}$

For this on-design case, the HTC along the X axis from the leading edge to the trailing edge, for 10, 25 and 50% span has been plotted.

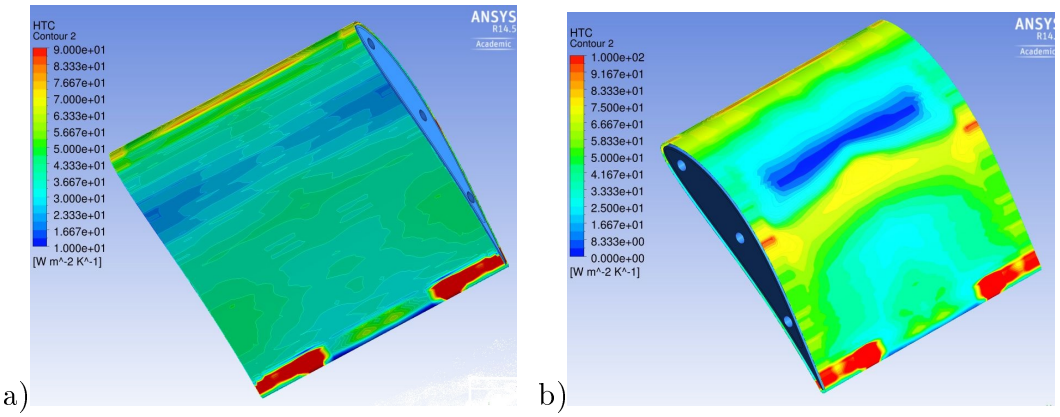

Figure 7.8: a) Pressure Side results b)Suction side results

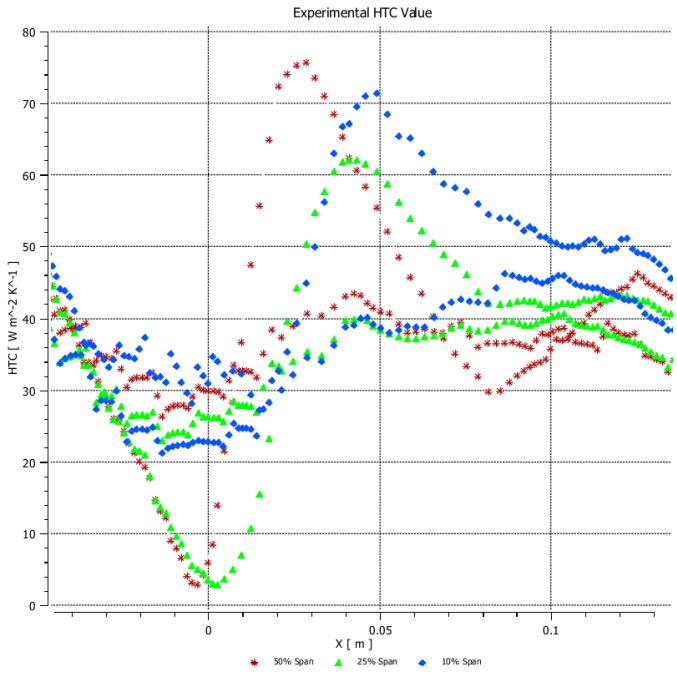

Figure 7.9: HTC along X axis for 10,25 and 50 % span

From the chart 7.9, we can see how the transition is very clear in the suction side, shown by the sudden increase in the HTC. Also we see how the pressure side HTC has a very uniform value.

7.3.5 On-Design: -25 º air inlet velocity: 30 $\frac{m}{s}$

In this case the shape of the HTC distribution also changes compared to the 100 % velocity case.

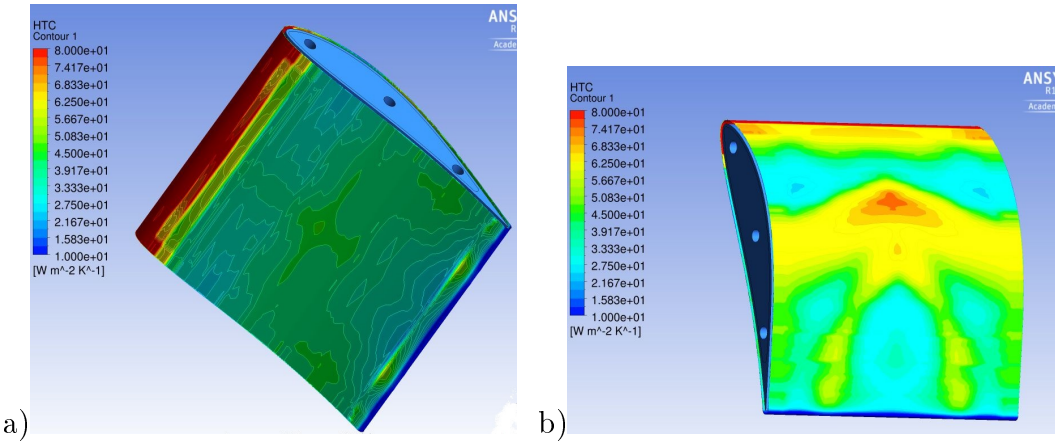

Figure 7.10: a) Pressure Side results b)Suction side results

7.4 Discussion and Comparison with CFD results

First of all, it is important to point out that in the HTC distribution we get some irregularities from CFX, this is mainly because the exportation from MatLab to fluent cannot fulfill the whole geometry of the surface. Also, Fluent uses some extrapolations to complete the temperature profile: this is made very clear especially in the leading and trailing edges of the vane.

7.4.1 CFD results

In the following figures, the simulated flow field for the on-design 100% velocity will be shown after having used two solving models for the transition. By looking at the stream lines. The turbulence model y k-w and with SST transition model we get some disturbance in the predicted flow. But when the transition model is $\gamma - \theta$ the flow exits perfectly the control volume with no disturbances.

a) 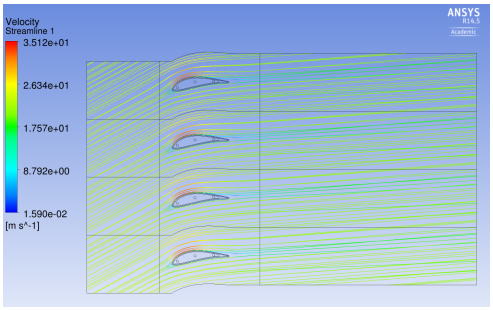

b) 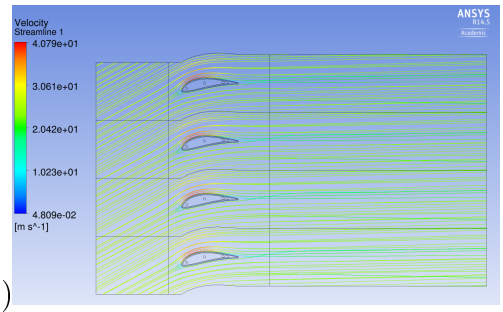

Figure 7.11: a) Stream lines using the SST model b)Stream lines using $\gamma - \theta$ model

In the figure 7.12 it is shown the predicted HTC distribution by this solution of the flow field for theses two transition models. It can be clearley seen how the distribution is much less complex than the experimental distribution and that the values than the CFD predict are not similar to the ones obtained in the experiment. Also the differences between the two transition models are big as it wouuld already be expected from the streamlines.

a) 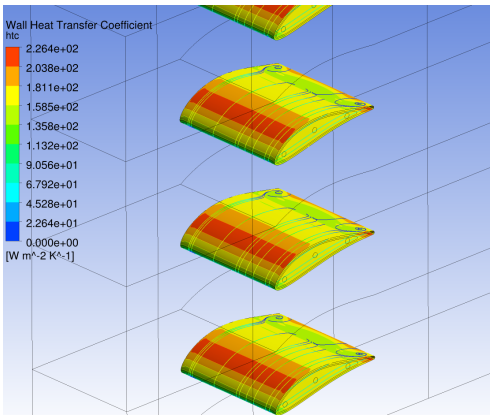

b) 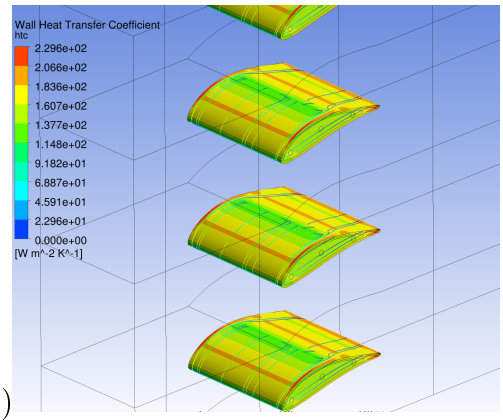

Figure 7.12: a) Computed HTC using the SST model b)Computed HTC using $\gamma - \theta$ model

Chapter 8

Conclusions

The main conclusion from the first part of the project (the investigation of IR transparent materials for our MWIR camera) is that Si is a material that works reasonably well in the range that our device needs. Therefore, after this work, it can be said that the implementation of Si in the lab rigs for future experiments is totally feasible. However, some additional experience with the window would help the work be more accurate in the future when working with Silicon.

The conclusion taken from the heat transfer experiment on the OGV is that experimental results are always needed in order to backup the results that can be obtained by computer simulation. In this specific work, we have seen how the HTC predicted by two different models differ in a very important way from the experimental distributions obtained.

Bibliography

[1] C. Arroyo Osso, (2009) *"Aerothermal Inestigation of an Intermediate Duct"*, Thesis for the Degree of Doctor of Philosophy, Chalmers University of Technology

[2] Borja M. Rojo Perez (2012) *"Experimental Heat Transfer Study in Intermediate Turbine Duct"*, Master's Thesis in Solid & Fluid Mechanics, Chalmers University of Technology

[3] Carlos Jimenez (2013) *"Experimental Heat Transfer Studies with infrared camera"*, Master's Thesis in Solid & Fluid Mechanics, Chalmers University of Technology

[4] Borja Rojo, Carlos Jimenez and Valery Chernoray (2013) *"Experimental Heat Transfer Study of Endwall in a Linear Cascade with IR Thermography"*

[5] Incropera, DeWitt, Bergman, Lavine (2007) *"Fundamentals of Heat and Mass Transfer"*, 6^{th} edition.

[6] J.P Holman, *"Heat Transfer"*, 10^{th} edition, McGraw Hill

[7] *Edmund*$^{(c)}$ *Optics* Digital Catalogue

[8] *Phoenix*^{TM} Camera System With RTIE. Version 120. Indigo Systems Corporation.

[9] Robert P. Madding, *"IR Window Transmittance Temperature Dependence"*, Infrared Training Center. FLIR Systems, Inc